Available online at www.sciencedirect.com

ScienceDirect
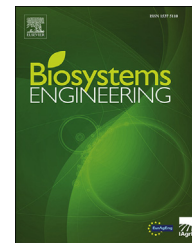
Research Paper

Numerical simulation approach to predict the abrasion rate of rice during milling

Xiangyi Meng [1], *Yanlong Han* [1], *Fuguo Jia* [*], *Peiyu Chen, Yawen Xiao, Shigang Bai, Hongwei Zhao*

College of Engineering, Northeast Agricultural University, Harbin, Heilongjiang, 150030, China

ARTICLE INFO

The effect of the rice movement and the forces acting on rice grains during abrasion in a mill is unclear limiting the development of rice milling machines. The aim of this work is to provide a numerical methodology for predicting the abrasion rate of rice to provide the basis for the design and use of rice mills and improving milling quality and efficiency. Here, the milling process was investigated experimentally in a laboratory using a vertical mill to identify the dominant abrasion mechanism and to the analyse of particle size distributions. In order to evaluate the abrasion rate, the effect of rotational speed of the roller shaft on the normal force and the sliding distance between particles and particle-geometry was examined using the discrete element method. Abrasion rate calculated according to the Archard abrasion equation from the simulation results and this agreed well with the experiment results thereby validating the feasibility of numerical-experimental approach. The relationship between rotational speed and abrasion rate was established based on polynomial fitting.

1. Introduction

Rice as a staple food is normally consumed in whole milled form (Mohapatra & Bal, 2007). Nutrients such as dietary fibres, essential amino acids, minerals, proteins and vitamins are present in the outer layers of the kernel and the germ (Samadder, Someswararao, & Das, 2017). *Under-milled* rice is rich in nutrition but has an inferior eating and optical qualities due to the residual bran layer. Whilst over milling will not only remove the bran layer of rice, it can considerably reduce its nutritional value and also cause broken grains (Roberts, 1979; Jung, Kim, & Kim, 2001). The essence of rice milling process is the interaction between particles and particle-geometry,

leading to the abrasion of the grain and removal of bran layer. Therefore, in order to control rice milling quality, and meet the needs of consumers for nutrition and taste, it is necessary to clarify the effects of operational factors to accurately predict rice abrasion rate.

The milling process is affected by a combination of rice properties and operating parameters as well as the geometry of the mill. For a given variety of rice with a specific mill, different milling qualities can be obtained by changing the operating parameters according to different requirements. Effects of the feed gate opening, clearance between rotor and milling bar, milling time, the mass of the sample being milled and mass within the milling chamber on milling quality have

---

Nomenclature

DEM	Discrete element method
F_{ntotal}	Normal total force (N)
F_{ttotal}	Tangential total force (N)
F_n	Normal contact force (N)
F_n^d	Normal damping force (N)
F_t	Tangential contact force (N)
F_t^d	Tangential damping force (N)
F_c	Coulomb friction force (N)
E^*	Equivalent Young's modulus (Pa)
G^*	Equivalent shear modulus (Pa)
R^*	Equivalent radius (m)
α	Normal overlap (m)
ε	Coefficient of restitution
S_n	Normal stiffness (N m^{-1})
m^*	Equivalent mass (kg)
S_t	Tangential stiffness (N m^{-1})
δ	Tangential overlap (m)
v_n^{rel}	Normal components of the relative velocity (m s^{-1})
v_t^{rel}	Tangential components of the relative velocity (m s^{-1})
F_c	Coulomb friction force (N)
μ_s	Coefficient of static friction
V	Abrasion induced volume fractional loss (m^3)
H	Material Hardness (MPa)
K	Dimensionless coefficient
PSD	Particle size distribution
CU	Coefficient of uniformity
CC	Coefficient of curvature
P	Porosity
N	Average number of particles in each region
V_r	Volume of each region (m^3)
V_p	Volume of each particle (m^3)
n	Rotational speed of roller shaft (rpm)
Ar	Abrasion rate (g s^{-1})

been studied by several researchers (Andrews, Siebenmorgen, & Mauromoustakos, 1992; Gujral, Singh, Sodhi, & Singh, 2002; Meng et al., 2019; Roberts & Wasserman, 1977). This research has concentrated on the influence of various parameters on final milling quality and tried to provide an optimal operating parameters empirically using design of experiments procedures. However, these results are based on experience and trial and error tests and are only suitable for the test machines used under a predetermined ranges of process parameters limiting the confidence and suitability of the guidelines produced when drastically different equipment configurations are used (Rosenbaum, Tan, Dummeldinger, Mitchell, & Engstrom, 2019). This is because this approach has difficulties in providing insights into the interaction between rice particles or particle-geometry during the milling process. In fact, it could be inferred that no matter how the operating conditions are changed, the abrasion of rice can be regarded as a change in the normal force and sliding distance which the rice grain is subjected to. However, the influence of these two parameters remains unclear.

Fortunately, recent advances in computer simulation technologies based on the discrete element method (DEM) have made it possible to obtain more detailed information. The flow process of rice particles in the mill can be simulated directly and detailed microscopic information such as velocity, compressive force and orientation angle can be obtained conveniently to determine the difference in movement characteristics under different milling conditions (Han et al., 2017; Zeng, Jia, Meng, Han, & Xiao, 2018). In order to reveal milling performance, collision energy is commonly selected (Weerasekara, Liu, & Powell, 2016; Cao et al., 2018). However, these results can only indirectly reflect on milling performance, which are difficult to provide quantitative guidance for practical production and application. Han et al. (2016) described how to find the appropriate micro indices from simulations such as collision energy, and flow velocity. Macro quality parameters were chosen from the experiments such as head rice yield and wear mass loss. Establishing the relationship between indices and parameters to connect simulation and experiment is practically useful. Therefore, it is necessary to make a connection between normal force, sliding distance and abrasion rate.

The main objective of this work was to determine the dominant mechanism of milling in a vertical mill. Also, a method to predict the abrasion rate of rice during milling, using a numerical-analytical approach according to the Archard abrasion equation was proposed. This has the potential to be used for the design, use and optimisation of rice mills.

2.   Materials and methods

2.1.   Experimental materials

Short grain of the Japonica type (Dongnong No. 429) provided by the rice processing laboratory of the Northeast Agricultural University (Harbin, China) was dehusked using a Satake rice dehusker (THU-35B type, Satake, Tokyo, Japan). After dehusking, brown rice was cleaned using sieves to remove all foreign matter and broken and immature grains. The initial moisture content of brown rice was 10.1 ± 0.3% (w.b.), which was determined using standard air oven method (AOAC, 1980). The optimal moisture content of brown rice for milling is recommended to be between 15 and 16% (w.b.) (Jia, Nan, & Bai, 2006). Therefore, brown rice samples were conditioned to a moisture content level of 15.5 ± 0.1% (w.b.), by adding a measured amount of distilled water, followed by thorough mixing, and sealing the samples in double polythene bags. The conditioned samples were kept at 5 ± 1 °C in a refrigerator for 7 d to allow uniform distribution of moisture throughout the sample (Vishwakarma, Shivhare, & Nanda, 2012).

2.2.   Milling process

A laboratory vertical circulation mill (SY95-PC+PAE5, Ssangyong Machinery Co., Korea) was used in this work (Fig. 1). It essentially consists of four parts: a feed hopper, a roller shaft with a screw and two convex ribs, an outlet and a milling
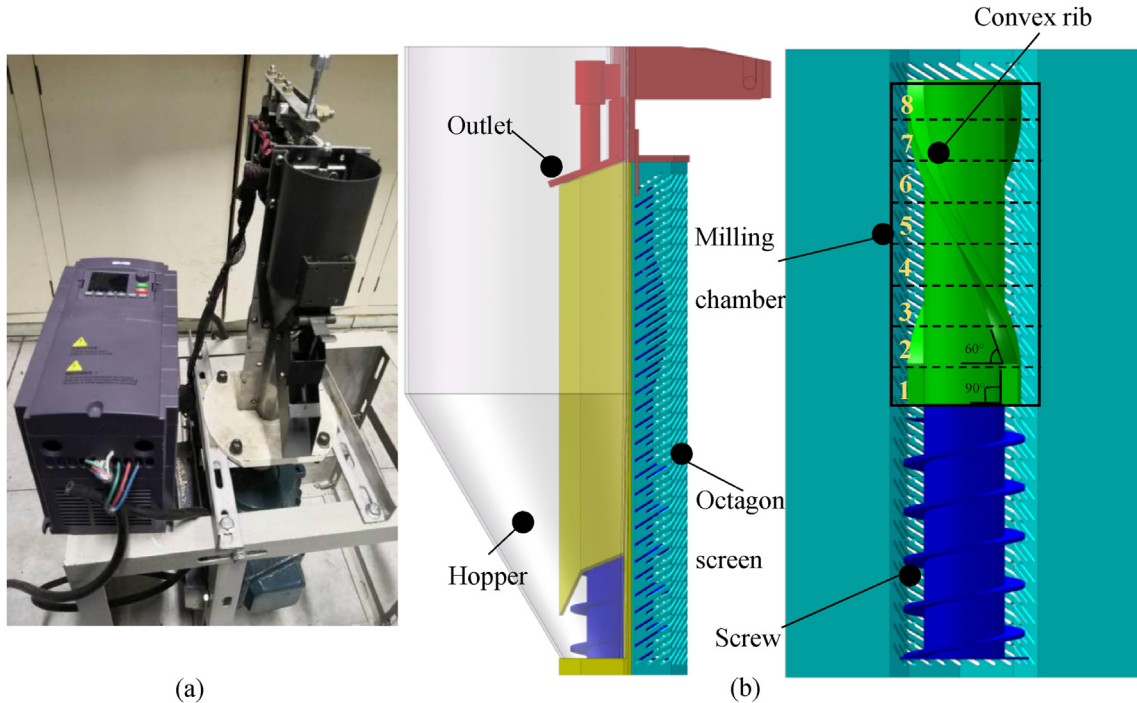
Fig. 1 – Configuration of the rice mill: (a) schematic diagram of the vertical rice mill used in experiments; (b) schematic diagram of the simplified key components used in the DEM simulations.

chamber surrounded by an octagonal rice screen. After obtaining the initial size distribution, 120 g of brown rice was fed into the hopper. The milling was performed for 60 s under the rotational speed of 1400 rpm. Under this condition, the milled rice can reach the standard quality, corresponding to the milling degree of 8%. Any further major change of grain size or a superior optical quality was determined as needing significantly longer time and more energy consumption. Following milling, the milled rice remained in the mill was discharged into a collection box to measure the size distribution. The fines produced not in the screen were specified as the bran layer and were not measured within the particle size distribution. However, some fines stayed in the collection bin and adhered to the collection bin and the internal walls of the milling chamber. Thus, each part of mill was cleaned using a soft brush after milling.

The size distribution of the rice was obtained by image analysis, which is generally considered to be a more objective, precise and reproducible method than manual measurement. Raw images of rice before and after milling were obtained. Half of the collected milled rice was spread onto a dark flat surface to ensure a fair contrast between the background and the white kernels. A reference object (15 × 15 mm rectangular paper strip) was also placed in the same image, along with the rice kernel. A cell phone camera fixed on a black box approximately at 0.15 m from the surface was used to take an image of rice kernels with the camera flash turned off. The initial image was then processed using Fiji software, which is an adaptation of Image J, open source software produced by the US National Institute of Health. It can swiftly measure the designated areas and return rice data such as major axis length. Details about the image processing steps in Fiji can be found in Bankole, Buckman,

Stow, and Lever (2019), and is not repeated here for brevity. The size distribution was presented as number fractions in a given size interval for comparison purposes. Symbols were plotted at the centre of each size interval, and sizes were based on the major axis of each rice grain.

3. Numerical modelling

3.1. DEM model

To evaluate effects of rotational speed of roller shaft on the normal force and sliding distance which rice particles are subjected was established using a DEM model and the abrasion rate was calculated. A Hertz–Mindlin no-slip model (Cundall & Strack, 1979) was employed to model each contact between particles or particle-geometry using the commercial package EDEM (DEM Solutions Ltd., Edinburgh, Scotland, UK).

The contact between any two solid spheres, is represented by the spring–dashpot system, which is also commonly referred to as the soft-sphere approach. In the normal direction, the spring and dashpot together define the normal total force (F_{ntotal}) given by:

$$F_{ntotal} = F_n + F_n^d = \frac{4}{3}E^*\sqrt{R^*\alpha^3} - 2\sqrt{\frac{5}{6}}\frac{\ln\varepsilon}{\sqrt{\ln^2\varepsilon + \pi^2}}\sqrt{S_n m^*}v_n^{rel} \qquad (1)$$

where E^* is the equivalent Young's modulus, R^* is the equivalent radius, and α is the normal overlap. ε is the coefficient of restitution. S_n is the normal stiffness. m^* is the equivalent mass. v_n^{rel} is the normal components of the relative velocity between particles.

In the tangential direction, the relative tangential velocity from the relative tangential motions over the contact behaves as an incremental spring that stores energy and represents the elastic tangential deformation of the contacting surfaces. The dashpot dissipates energy from the tangential motion and models the tangential plastic deformation of the contact. In addition, the total tangential force (F_{ttotal}) is limited by the Coulomb's law of friction (Cleary, 1998).

$$F_{ttotal} = \begin{cases} \mathbf{F}_t + \mathbf{F}_t^d = -S_t\delta - 2\sqrt{\dfrac{5}{6}} \ \dfrac{\ln\varepsilon}{\sqrt{\ln^2\varepsilon + \pi^2}}\sqrt{S_t m^*}v_t^{rel}, \\[2mm] \qquad \|\mathbf{F}_t + \mathbf{F}_t^d\| \leq \|\mathbf{F_c}\| \\[2mm] \mathbf{F_c} = \mu_s \mathbf{F}_n, \|\mathbf{F}_t + \mathbf{F}_t^d > \|\mathbf{F_c}\| \end{cases} \quad (2)$$

where S_t is the tangential stiffness, δ is the tangential overlap. v_t^{rel} is the tangential components of the relative velocity. $\mathbf{F}_c$ is the Coulomb friction force. μ_s is the coefficient of static friction. Some detailed definitions of above parameters are listed in Table 1.

3.2. Simulation condition

The schematic of the mill used in the simulation process was the same as that used in the milling experiment although only the key components were retained to simplify the modelling and increase computational efficiency, as shown in Fig. 1 (b). A multi-sphere model with axis-symmetric ellipsoid of a 6.6 mm long axis and a 2.2 mm short axis was employed for the representation of brown rice, as shown in Fig. 2 (b). Detailed geometric parameters, operating conditions and material properties used in this simulation are summarised in Table 2. These material and geometry parameters were referred to in our previous literature (Cao et al., 2018; Han et al., 2016; Han, Jia, Tang, Liu, & Zhang, 2014; Jia et al., 2014).

Rice particles were fed into the hopper randomly with the roller shaft rest at the beginning of a simulation. After the required particles were generated they remained stable at the bottom of the hopper, the roller shaft begins to rotate at a given speed to bring the rice particles moving into the milling chamber. All the results were analysed after 3 s, when the system reached the macroscopically dynamic steady state. The steady state here was determined when the time averaged velocity for all particles just slightly fluctuates around its mean value, as shown in Fig. 3. Model reliability was proven by comparing power values and the dimensionless residence time distribution obtained in the DEM simulation

with those of the physical experiment in our previous work (Cao et al., 2018; Han et al., 2016) and this is not repeated here for brevity.

3.3. Abrasion model

When particles are subjected to low velocity contacts or undergo rubbing between surfaces, the materials undergo surface abrasion, leading to the production of very fine particles. Whilst at higher velocity, attrition is controlled by particle fragmentation in which the particles breaks into two or more fragments (Riley, Siriwardane, & Poston, 2020). Generally, abrasion, the former type of attrition, is more likely to occur in rice milling. For these abrasion sources, various models have been presented to relate the measured abrasion rate to the variables. The abrasion models in the literature can be categorised as (1) empirical, (2) contact-mechanics based, and (3) material failure mechanism (Bayham, Breault, & Monazam, 2016). The classical Archard equation based on contact-mechanics has been widely used to calculate abrasion (Jafari & Abbasi Hattani, 2020; Xu, DeCroix, & Sun, 2014).

$$V = K\frac{F_n \Delta s}{H} \quad (3)$$

where V is the abrasion induced volume fractional loss, H is the material hardness. The dimensionless coefficient for rice, K, which was approximately 0.04 based on the research of Mohapatra and Bal (2004). The hardness, H, of a material is usually considered to be its resistance to local deformation, can be obtained from the load-depth curve. The hardness for the rice was measured to be approximately 50 MPa (Zhang, Zhao, Guo, & Han, 2010). Fn is the normal force, and Δs is the sliding distance which is calculated based on the relative tangential displacement between two particles or particle-geometry in contact using DEM simulation. It should be pointed that the abrasion based on the Archard equation only was calculated here, assuming the velocity in the milling chamber is reasonably low enough to prevent other attrition modes, such as chipping or fragmentation. An ongoing rice impact test showed that the rice broke only when the impact velocity was >10 m s^{-1}. Figure 4 shows the relative normal velocity obtained from a DEM simulation concentrates near 0.2 m s^{-1}, which is far less than the critical value of 10 m s^{-1}, providing a basis for our hypothesis. In order to identify the dominant mechanism accurately, rice size reduction of the milling process was analysed in the following part.

4. Experimental results

The main mechanism of milling can be determined by estimating the size distribution following milling. Therefore, the particle size distribution of rice samples before and after milling was determined. It can be seen from Fig. 5, the peak of the particle size distribution (PSD) shifted from 6 to 7 to 5−6 mm after milling. There was only a small shift of the main peak with no peak broadening. Monazam, Galinsky, Breault, and Bayham (2018) pointed out that when no peak broadening is observed this is a sign that abrasion is the primary

---

Table 1 − The equations of parameters used in the contact model.
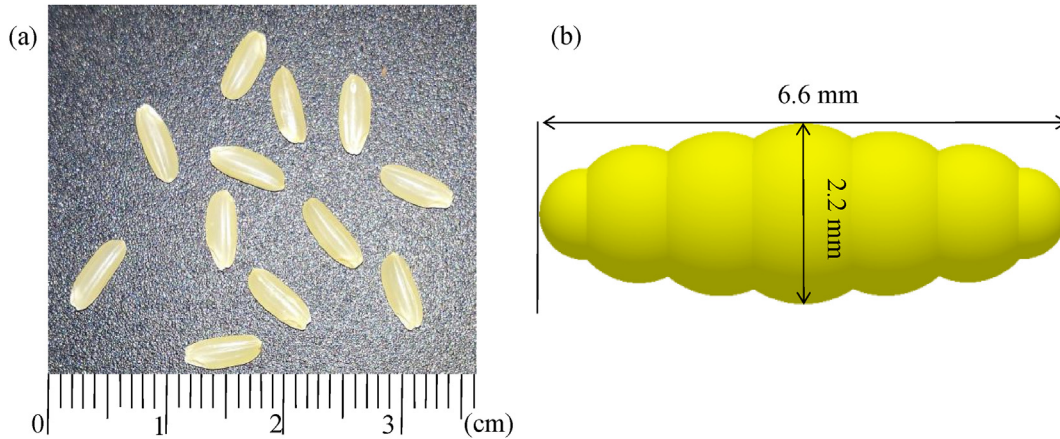
	Symbol	Equation
Normal stiffness	S_n	$2E^*\sqrt{R^*\alpha}$
Tangential stiffness	S_t	$8G^*\sqrt{R^*\delta}$
Equivalent Young's modulus	E^*	$\dfrac{1}{E^*} = \dfrac{(1-v_i^2)}{E_i} + \dfrac{(1-v_j^2)}{E_j}$
Equivalent radius	R^*	$\dfrac{1}{R^*} = \dfrac{1}{R_i} + \dfrac{1}{R_j}$

Where G^*: equivalent shear modulus; v_i, v_j: Poisson's ratio; R_i, R_j: radius of each sphere in contact.

Fig. 2 – Geometry of a typical brown rice particle: (a) photographs of brown rice; (b) multi-sphere model of rice particles as used in the DEM simulations. (For interpretation of the references to colour in this figure legend, the reader is referred to the Web version of this article.)

Table 2 – Geometry parameters and physical parameters used in the simulation.

Type	Parameters	Value
Hopper	Diameter $D_h \times$ height L_h (mm)	82×190
Roller shaft	Screw pitch, L_s (mm)	12
	Screw diameter, D_s (mm)	30
	Shaft diameter, D_s (mm)	20
	Shaft height, L_s (mm)	140
	Convex rib height $H_c \times$ width $D_c \times$ thickness L_c (mm)	$80 \times 3.5 \times 4.2$
	Rotational speed, ω (rpm)	700, 1050, 1400
Octagon rice sieve	Side length, w (mm)	14.8
Rice particle	Density, ρ_p (kg m^{-3})	1550
	Poisson ratio, ν_p	0.25
	Shear modulus, G_p (Pa)	1×10^6
	Number of particles	6000
Mill	Density, ρ_m (kg m^{-3})	7800
	Poisson ratio, ν_m	0.3
	Shear modulus, G_m (Pa)	7×10^8
Particle–particle	Restitution coefficient, e_{pp}	0.68
	Coefficient of static friction, μ_{spp}	0.15
	Coefficient of rolling friction, μ_{rpp}	0.01
Particle-mill	Restitution coefficient, e_{pm}	0.68
	Coefficient of static friction, μ_{spm}	0.1
	Coefficient of rolling friction, μ_{rpm}	0.01
Simulation	Time step, Δt (s)	1.5×10^{-5}

mechanism of attrition. Therefore, through a macroscopic observation of PSD of milled rice, it can be stated the grain size reduction was dominated by abrasion under the tested conditions.

To quantitatively analyse the distribution characteristics of rice particle after milling, the coefficient of uniformity and coefficient of curvature were selected. The coefficient of uniformity (CU) is a numerical estimate of how well a particle sample is graded by measuring the particle size range (Chourasia & Alappat, 2018). The CU value is generally found to be larger than 1. The more it closes to 1, the more uniform the rice sample is. The CU is given by the ratio of D_{60} and D_{10} sizes.

$$CU = D_{60}/D_{10} \qquad (4)$$

where D_{60} and D_{10} are the grain size indicated by the cumulative undersize distribution curve at the 60% and 10% passing level, respectively.

While the shape of the particle size distribution curve is represented by the coefficient of curvature CC. When the CC is in the range of 1–3, it means the particle size distribution is continuous without absence of certain size, indicating the size of particle reduces gradually, instead of the occurrence of fragmentation. The CC is given by:

$$CC = (D_{30})^2 / (D_{60}D_{10}) \qquad (5)$$

To calculate D_{10}, D_{30} and D_{60}, the cumulative undersize distribution curve has to be obtained first. As shown in Fig. 6, the cumulative undersize distribution curve of the rice migrates towards small sizes demonstrating a reduction in rice
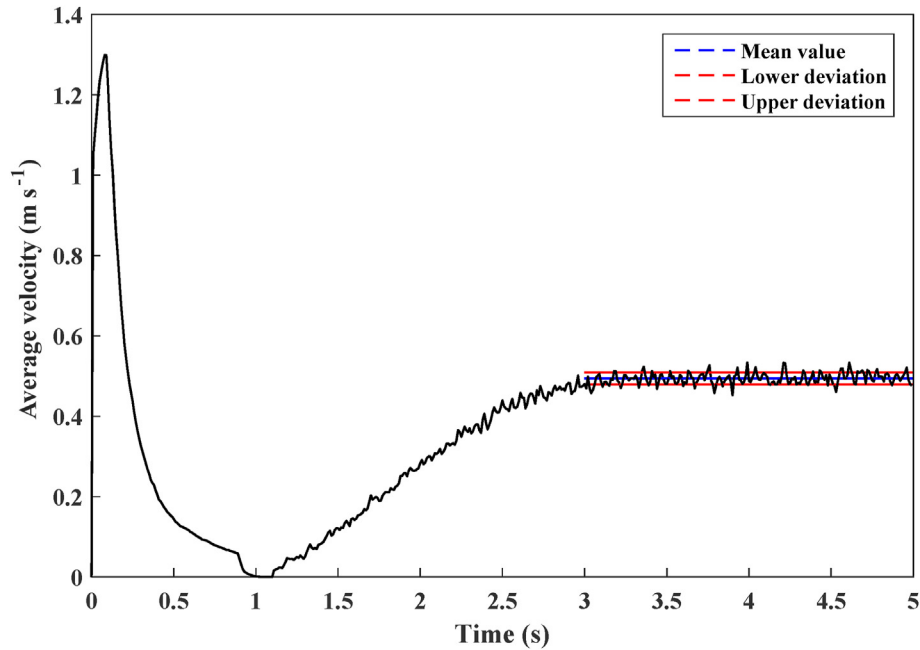
Fig. 3 − DEM predictions of the variation of average velocity of particle in the mill with time under the rotational speed of 1400 rpm.
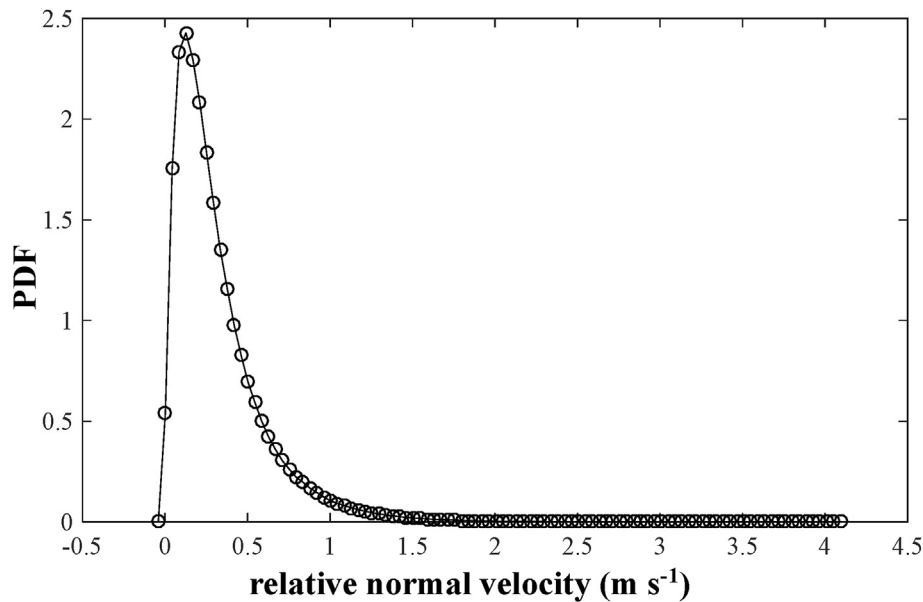

Fig. 4 − DEM predictions of the probability density distribution of relative normal velocity under the rotational speed of 1400 rpm.

size. Figure 7 shows that the coefficient of uniformity (CU) and coefficient of curvature (CC) increases to 1.75 and 1.53 respectively, after milling. Based on the characteristics of these two coefficients, the result suggests that the rice particles of different size ranges are produced in the operation. More importantly, rice size gradually decreases, indicating that abrasion played a dominant role in the mill under the current geometry and operating conditions. Therefore, the Archard equation was assumed to be suitable to investigate the milling process of rice.

5. Simulation results and discussion

5.1. Effect of rotational speed on contact characteristics

In order to obtain a detailed microscopic contact characteristics of rice particles, the milling chamber is divided into eight equal parts which are all the same length as 10 mm from the beginning of the convex rib to the end, as shown in Fig. 1 (b). Note that all the following analysis is done in the milling
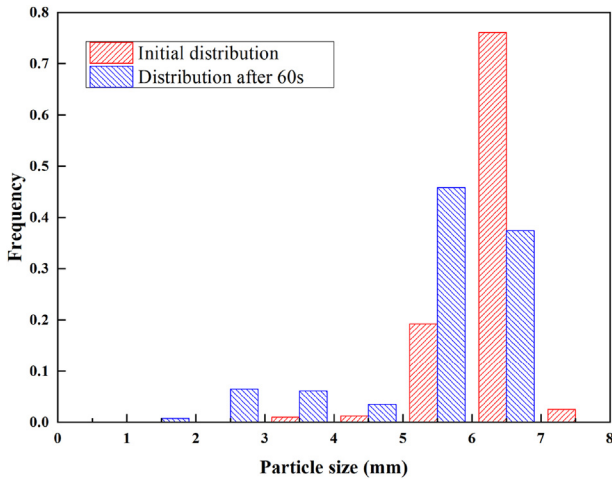
Fig. 5 – Experimental results of the particle size distributions before and after milling under rotational speed of 1400 rpm.
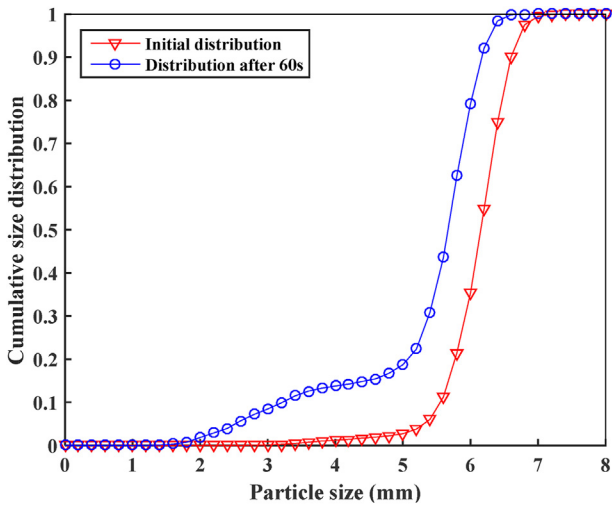
Fig. 6 – Experimental results of the cumulative particle size distribution before and after milling under rotational speed of 1400 rpm.

chamber. The abrasion of particle is from the interaction between particles, particle-roller shaft as well as particle-screen. To clearly quantify the difference, the normal force and sliding distance of the three types of contact are obtained and presented respectively.

5.1.1.   Contact between particles

Figure 8 shows that the normal force per contact between particles gradually decreases from region 1 to 8. It can be contributed to the difference of porosity in the milling chamber from the bottom to the outlet due to the structure of the vertical mill, as shown in Fig. 9. The porosity increases linearly under different regions. It is calculated as follows (Liu et al., 2019):

$$P = \frac{V_r - N \times V_p}{V_r} \qquad (6)$$

where P, N are the porosity and average number of particles in each region respectively. V_r is the volume of each region. V_p is the volume of each particle.

Because of gravity, the particle stream was relatively dense in the lower part of the milling chamber, therefore interaction between particles was stronger in that region. Compared with the lower region, the normal force between two particles was reduced. It was primarily due to two aspects. Particles in the upper part of the mill gain potential energy in exchange of kinetic energy, causing the interactions between particles to weaken. However, as particles became loosely packed, the longer distance between particles resulted in a reduction in the normal force. The data in Fig. 8 also indicates that there was a marked increase in the extent of the normal force when the rotational speed of the roller shaft was increased from 700 rpm to 1400 rpm. The increase in the rotational speed resulted in particles with higher kinetic energy and thus greater contact force. The sliding distance between particles decreased gradually from region 1 to region 8. This can be attributed to particles in the lower part being densely packed, resulting in the contact time and relative velocity being greater.

5.1.2.   Contact between particle and roller shaft

The key part in the milling chamber was the rotating roller shaft with two convex ribs. Figure 10 shows the normal force between particle and roller shaft decreases sharply in the first two regions, and it gradually approached a constant value. Except that the gravity makes particles become dense at the bottom, the structure of the convex rib also plays an important role. The design of the rotational direction of convex ribs was in the opposite direction from screw cutting edges. When rice particles entered the milling chamber, the flow upward ability of the particles was restricted, causing a reduced porosity in the lower part of the milling chamber. In addition, the helical inclination angle of rib was 90 in the first region while in the following region was a fixed value of 60, as can be seen in Fig. 1 (b). Different inclination angle of convex rib will cause the variance of contact area and time between the particle and roller shaft. Han et al. (2020) once pointed out the larger contact area corresponding to a larger contact force during an impact experiment. Therefore, the design of inclination angle of 90 must have produced the relatively large normal force, causing the rapid initial abrasion of brown rice. Our previous research discovered the height of convex ribs has a vital influence on the motion of axial and radial direction further causing the difference in milling performance in a horizontal rice mill (Zeng et al., 2019). Therefore, the appropriate design of convex rib structure must be benefit for improving the quality of milled rice. Figure 10 also shows that the increase in the rotational speed of the roller shaft obviously generates greater normal force on the particle. Compared with that between particles, the normal force per contact between particle-roller shaft was almost twice larger, indicating a more rapid abrasion rate.

5.1.3.   Contact between particle and screen

The interaction between particle and screen is shown in Fig. 11. It can be seen that the normal force gradually
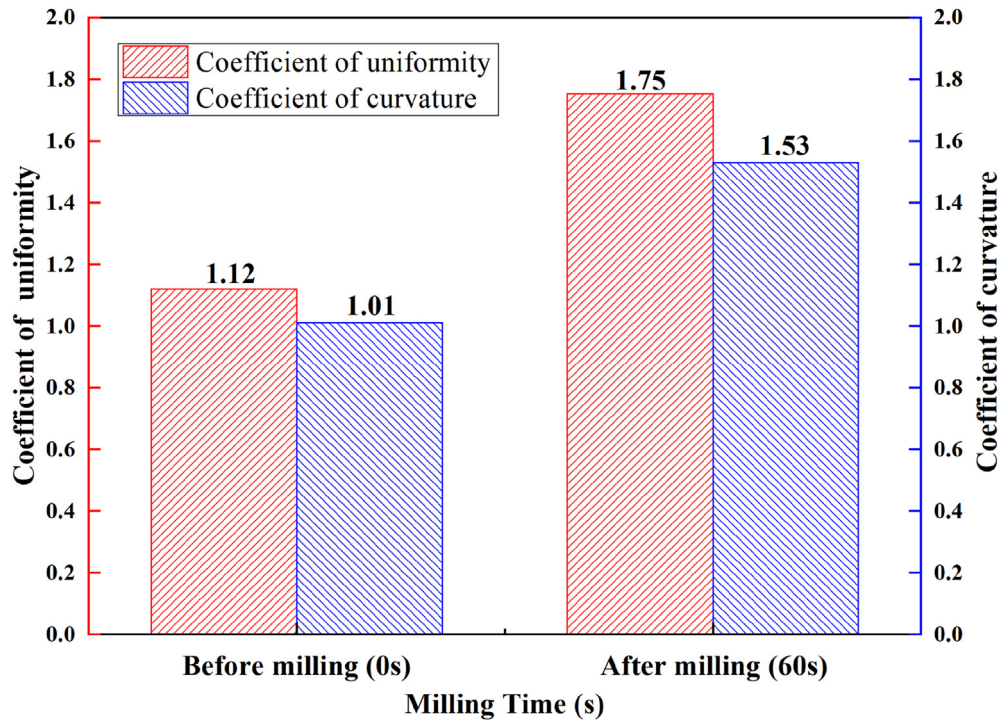
Fig. 7 — Experimental results of Coefficient of uniformity (CU) and coefficient of curvature (CC) before (0s) and after milling (60s) under rotational speed of 1400 rpm.
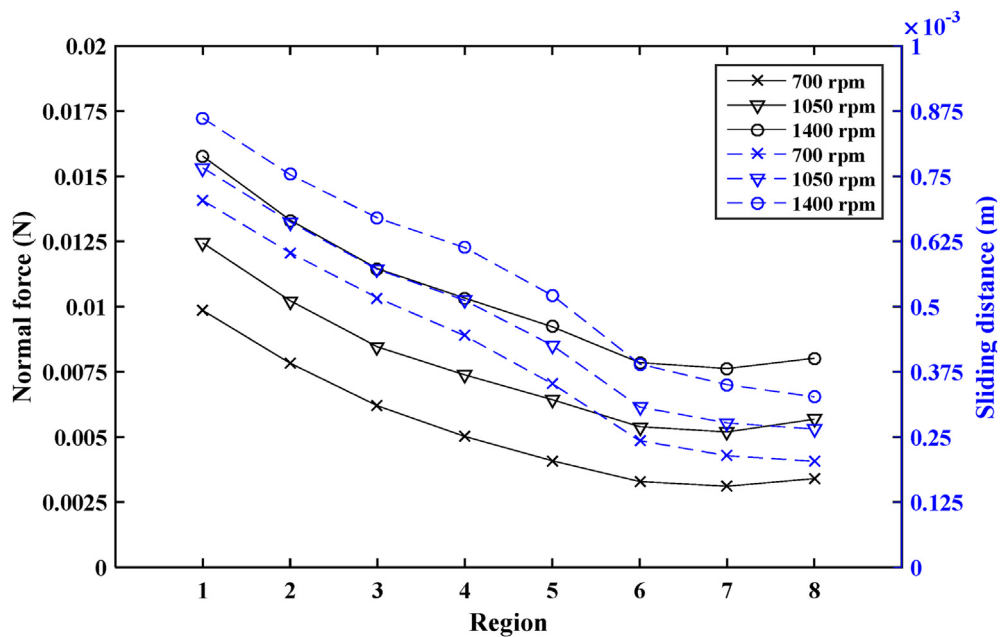

Fig. 8 — DEM predictions of normal force and sliding distance per contact between particle–particle under different rotational speeds.

decreases in the lower half of the whole milling chamber. While in the upper part, the normal force is almost constant. The result shows that the abrasion is more likely to occur at the bottom. The strength of the interaction between particle and screen can be intuitively reflected by the pressure sensitive paper, which is widely used to determine contact pressure profiles in many applications. Since the octagonal screen is axisymmetric along the axis of the roller shaft, pressure sensitive paper which covering 1/2 of the rice screen was enough to analysis the pressure distribution. After the rice mill was taken apart, a white paper was firstly attached to the inner wall of the screen. Then the two ends of the pressure paper
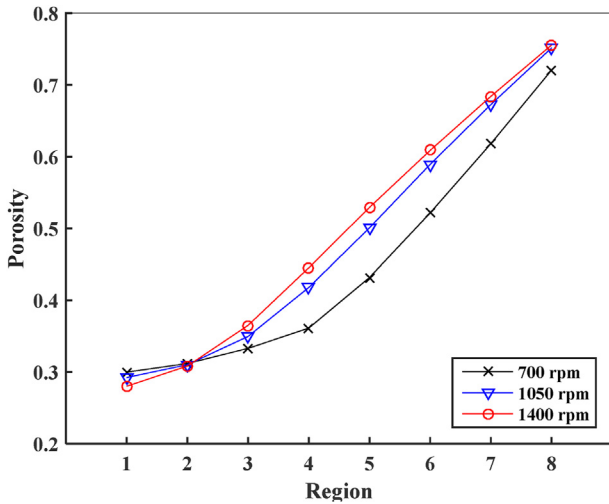
Fig. 9 — DEM predictions of porosity of different regions in the milling chamber under different rotational speeds.

were glued onto the white paper. After reassembling the machine for milling, the paper was carefully taken out of the milling chamber.

Figure 12 indicates that there is a distinct pressure gradient caused by the contact of the rice and screen. The high pressure regions are presented in the lower half of the paper, indicating the abrasion of particle was severe. The results corresponded well for the trend obtained in Fig. 11, indirectly validating the reliability of the DEM simulation results. Meanwhile, Fig. 12 also shows a darker colour at the corner as the dashed red line shown, demonstrating the corner is subjected to more severer abrasion. In summary, the uneven distribution of pressure will result in milling non-uniformity

and reducing the utilization of rice screen. To avoid local failure and extend service life of a rice screen, two effective methods are commonly adopted. One is to turn the screen by 180° alongside the radial direction after milling for a certain period of time. The other method is adjusting the structure of the feed screw to enable the particles fed into the milling chamber a smoother approach.

5.1.4. Contact number

During a whole milling process, it is the per contact intensity and the number of contacts that together determine the abrasion. Therefore, it is necessary to discuss the variation of the contact number in the milling chamber, divided in particle–particle, particle-roller shaft and particle-screen, as function of the rotational speed. It can be seen in Fig. 13, the number of particle–particle contacts is significantly higher than the number of particle-shaft and particle-screen contacts. While the contacts between particle and roller shaft are the least. The reason for the differences is that the number of particle–particle contacts is proportional to the number of particles in the milling chamber, whilst the number of particle-shaft and particle-screen contacts are proportional to the surface area of the shaft and screen, respectively. In addition, due to the action of centrifugal force, particles are more likely to be in contact with the screen than the roller shaft. Meanwhile, the reduction in the number of contacts between particles is more obvious compared with the other two kinds of contacts, especially in upper part of the milling chamber. The number of contacts between particle and shaft hardly changed in the different regions. Rotational speed had a strong effect on the lower part for the contact number between particles. By contrast, the number of particle-shaft and particle-screen contacts was only a weak function of rotational speed.
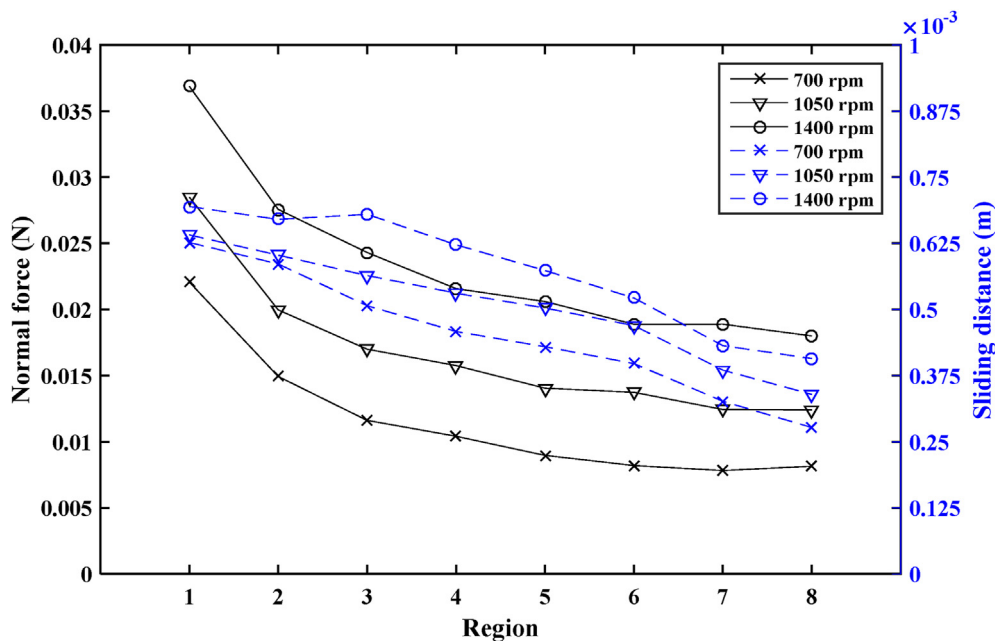

Fig. 10 — DEM predictions of normal force and sliding distance per contact between particle-roller shaft under different rotational speeds.
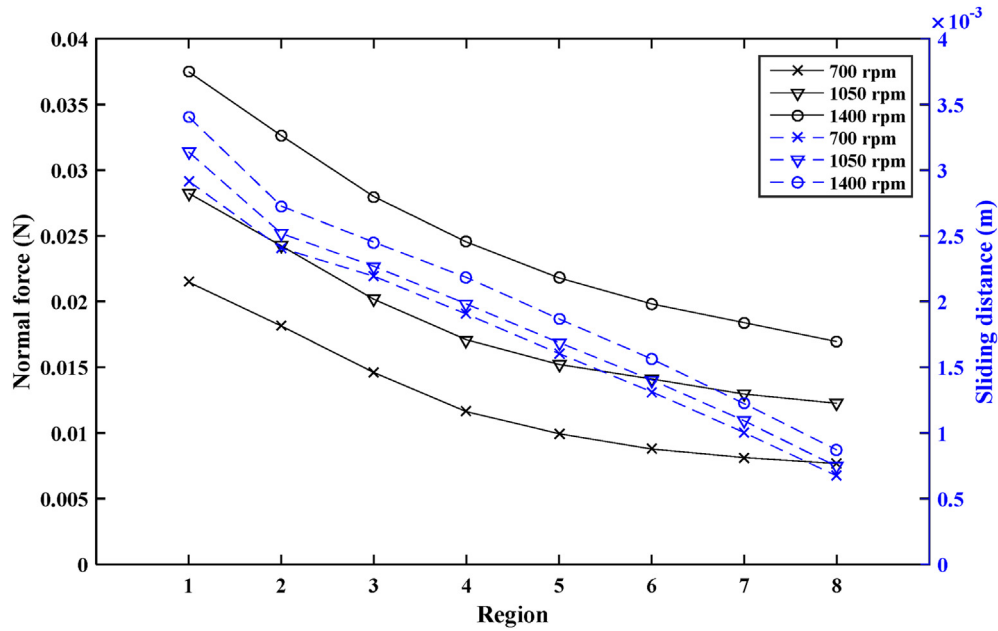
Fig. 11 — DEM predictions of normal force and sliding distance per contact between particle-screen under different rotational speeds.
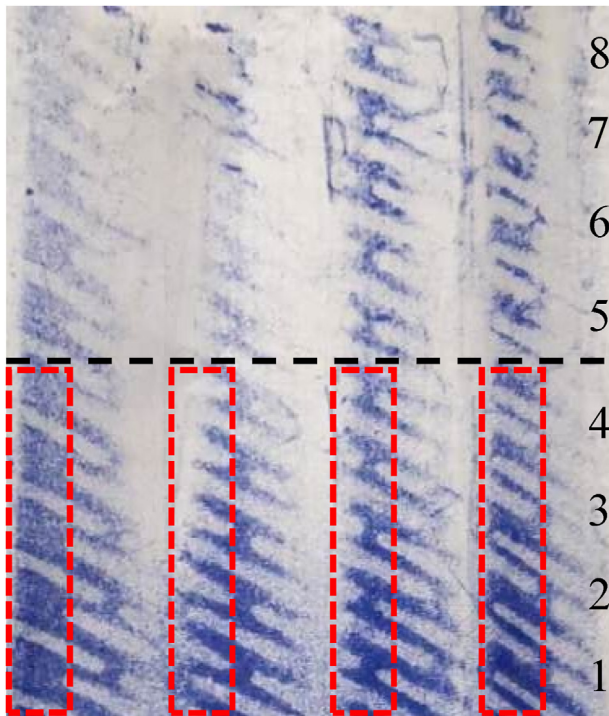

Fig. 12 — Pressure paper pattern under the rotational speed of 1400 rpm from milling experiment.

Fig. 13 — DEM predictions of the effect of rotational speed on the contact number between particles (PP), particle-screen (PS) and particle-roller shaft (PR) in different regions of milling chamber.

5.2.   *Effect of rotational speed on abrasion rate*

The effect of rotational speed on the normal force, sliding distance and contact number have thus been discussed. Applying the simulation results to the Archard equation the abrasion for each contact in the milling chamber can be calculated. Tot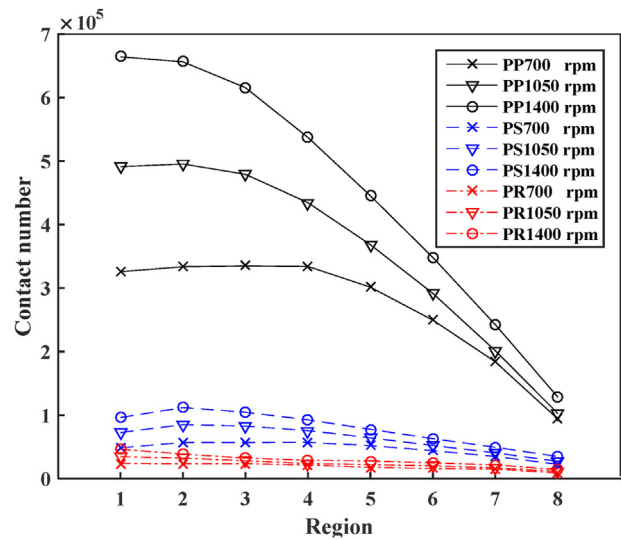al mass loss per second, abrasion rate, is calculated as the sum of abrasion volume of contacts multiplied by rice density. It is worth noting that the abrasion mass of particle—particle contacts double since both rice grains were abraded during such contacts.

Figure 14 shows the abrasion rate under different rotational speeds. It is divided in particle—particle and particle-geometry which includes the particle-roller shaft and particle-screen. The abrasion caused by the contact between particles is a little higher than that caused by the contact between particle and geometry. It can be seen the total abrasion rate increased more rapidly in the speed range 1050 rpm—1400 rpm than in the
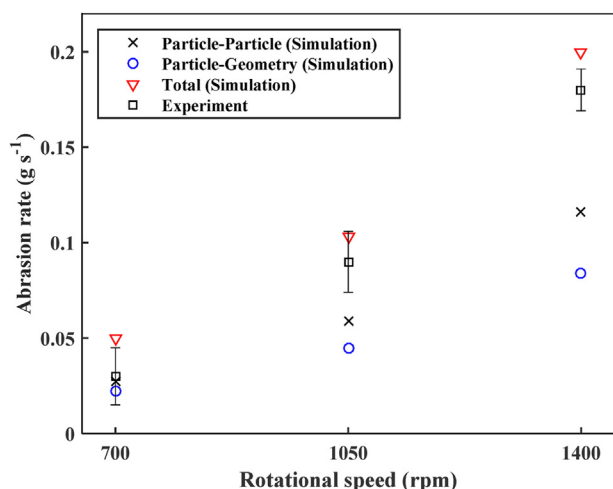
Fig. 14 – **Abrasion rate as a function of the rotational speed observed from experiments and predicted by DEM simulations.**

range 700 rpm–1050 rpm, indicating that increasing the rotational speed obviously increases abrasion rate.

According to the above analysis, in order to estimate the abrasion rate (Ar) as a function of the rotational speed (n) under the tested conditions, a relationship was formulated by the method of polynomial fitting, as given below:

$$Ar = p_1 n + p_2 \tag{7}$$

Here, p_1 and p_2 are two fitting coefficients. Based on the above results, they are 2.147×10^{-4} and -0.1077, respectively. The R^2 value is 0.973 for the model, indicating the fitting precision is higher.

6.   Discussion

The comparison of the abrasion rate obtained from numerical analysis and experimental results with error bar is presented in Fig. 14. Although, experimental validation has verified the precision of the proposed numerical-analytical method to a certain extent, the simulation results in a slightly over-estimated abrasion rate. The main causes of discrepancy between the numerical analysis and experimental results are discussed below.

In the simulation, the rice models are all in the same size and shape, but that is different in the experiment. In addition, the rice gradually becomes glossy causing reduced abrasion during further milling. It means the abrasion coefficient K of the Archard equation may change slightly with abrasion time. Based on the research of Mohapatra and Bal (2004), K was regarded as a constant in the present study. However, if a more accurate wear coefficient is required, a single particle abrasive test should be conducted. A device commonly used in chemical mechanical polishing, which essentially consists a load plane and rotating abrasive base plate, can be used a good reference (Lijesh & Khonsari, 2020; Lin, Gao, Li, & Yu, 2019). When the normal force and sliding distance acting on the rice grain are set, the amount of wear is obtained by weighing,

thus the wear coefficient can be calculated. Our research team is trying to build a device such as this which is suitable for single rice abrasion detection.

Also, as more attention is being paid to healthy eating, the processing of embryo rice with germ has become an important issue in current rice milling research (Yan, Hong, & Chung, 2005). The nutritional germ located in the one end of rice should be preserved intact during milling. Thus, the lateral sides of rice contact with the mill unit are important for this purpose. Common rice mills cannot meet this requirement due to the rice grains randomly contacting with each other due to the geometry of the milling chamber. Flat-belt type polishing devices can mill rice without destroying the germ due to the rice lying on the abrasive plate. This technique could provide the foundation of a design of a new type of rice milling machine, similar to a flat belt mill, which may contribute to the design of an important rice processing machine.

7.   Conclusions

The rice milling process was investigated combining the experiment and DEM simulation. The predominate mechanism of milling was abrasion in the vertical mill under the tested condition by analysing the milled particle size distribution. Then effects of rotational speed of roller shaft on the interaction between particles and particle-geometry were discussed. The abrasion rate predicted according to the Archard abrasion equation based on the simulation results agreed well with the experiment results, indicating it is an effective method to predict the abrasion rate in a rice mill. Finally, the relationship between rotational speed and abrasion rate was established based on the method of polynomial fitting.

Declaration of competing interest

The authors declare that they have no known competing financial interests or personal relationships that could have appeared to influence the work reported in this paper.

Acknowledgements

REFERENCES

Andrews, S. B., Siebenmorgen, T. J., & Mauromoustakos, A. (1992). Evaluation of the McGill No.2 rice miller. *Cereal Chemistry Journal, 69*(1), 35–43.

AOAC. (1980). *Official methods of analysis* (13th ed.). Arlington, Va: AOAC.

Bankole, S. A., Buckman, J., Stow, D., & Lever, H. (2019). Grain-size analysis of mudrocks: A new semi-automated method from SEM images. *Journal of Petroleum Science and Engineering, 174*, 244–256. https://doi.org/10.1016/j.petrol.2018.11.027

Bayham, S. C., Breault, R., & Monazam, E. (2016). Particulate solid attrition in CFB systems – an assessment for emerging technologies. *Powder Technology, 302*, 42–62. https://doi.org/10.1016/j.powtec.2016.08.016

Cao, B., Jia, F., Zeng, Y., Han, Y., Meng, X., & Xiao, Y. (2018). Effects of rotation speed and rice sieve geometry on turbulent motion of particles in a vertical rice mill. *Powder Technology, 325*, 429–440. https://doi.org/10.1016/j.powtec.2017.11.048

Chourasia, S., & Alappat, B. J. (2018). Effects of various parameters on the attrition of bed material in a recirculating fluidized bed with a draft tube. *Particuology, 38*, 61–70. https://doi.org/10.1016/j.partic.2017.05.011

Cleary, P. W. (1998). Predicting charge motion, power draw, segregation and wear in ball mills using discrete element methods. *Minerals Engineering, 11*(11), 1061–1080. https://doi.org/10.1016/s0892-6875(98)00093-4

Cundall, P. A., & Strack, O. D. L. (1979). A discrete numerical model for granular assemblies. *Géotechnique, 29*(1), 47–65. https://doi.org/10.1680/geot.1980.30.3.331

Gujral, H. S., Singh, J., Sodhi, N. S., & Singh, N. (2002). Effect of milling variables on the degree of milling of unparboiled and parboiled rice. *International Journal of Food Properties, 5*(1), 193–204. https://doi.org/10.1081/JFP-120015601

Han, Y., Jia, F., Tang, Y., Liu, Y., & Zhang, Q. (2014). Influence of granular coefficient of rolling friction on accumulation characteristics. *Acta Physica Sinica, 63*(17), 2–8. https://doi.org/10.7498/aps.63.174501

Han, Y., Jia, F., Zeng, Y., Jiang, L., Zhang, Y., & Cao, B. (2016). Effects of rotation speed and outlet opening on particle flow in a vertical rice mill. *Powder Technology, 297*, 153–164. https://doi.org/10.1016/j.powtec.2016.04.022

Han, Y., Jia, F., Zeng, Y., Jiang, L., Zhang, Y., & Cao, B. (2017). DEM study of particle conveying in a feed screw section of vertical rice mill. *Powder Technology, 311*, 213–225. https://doi.org/10.1016/j.powtec.2017.01.058

Han, Y., Zhao, D., Jia, F., Qiu, H., Li, A., & Bai, S. (2020). Experimental and numerical investigation on the shape approximation of rice particle by multi-sphere particle models. *Advanced Powder Technology, 31*(4), 1574–1586. https://doi.org/10.1016/j.apt.2020.01.025

Jafari, A., & Abbasi Hattani, R. (2020). Investigation of parameters influencing erosive wear using DEM. *Friction, 8*(1), 136–150. https://doi.org/10.1007/s40544-018-0252-4

Jia, F., Han, Y., Liu, Y., Cao, Y., Shi, Y., Yao, L., et al. (2014). Simulation prediction method of repose angle for rice particle materials. *Transactions of the Chinese Society of Agricultural Engineering, 28*(11), 189–195. https://doi.org/10.3969/j.issn.1002-6819.2014.11.031

Jia, F., Nan, J., & Bai, S. (2006). Study on the relationship between the moisture content of rice and milling characteristics. *Journal of Northeast Agricultural University, 37*(5), 665–668. https://doi.org/10.19720/j.issn.1005-9369.2006.05.019

Jung, K. P., Kim, S. S., & Kim, K. O. (2001). Effect of milling ratio on sensory properties of cooked rice and on physicochemical properties of milled and cooked rice. *Cereal Chemistry, 78*(2), 151–156. https://doi.org/10.1094/cchem.2001.78.2.151

Lijesh, K. P., & Khonsari, M. M. (2020). Characterization of abrasive wear using degradation coefficient. *Wear, 450–451*, 203220. https://doi.org/10.1016/j.wear.2020.203220

Lin, Z., Gao, B., Li, X., & Yu, K. (2019). Effect of abrasive grain size on surface particle deposition behaviour of PTFE/bronze composites during abrasive wear. *Tribology International, 139*, 12–21. https://doi.org/10.1016/j.triboint.2019.06.027

Liu, H., Jia, F., Xiao, Y., Han, Y., Li, G., Li, A., et al. (2019). Numerical analysis of the effect of the contraction rate of the curved hopper on flow characteristics of the silo discharge. *Powder Technology, 356*, 858–870. https://doi.org/10.1016/j.powtec.2019.09.033

Meng, X., Jia, F., Xiao, Y., Han, Y., Zeng, Y., & Li, A. (2019). Effect of operating parameters on milling quality and energy consumption of brown rice. *Journal of Food Science & Technology, 56*(2), 674–682. https://doi.org/10.1007/s13197-018-3522-2

Mohapatra, D., & Bal, S. (2004). Wear of rice in an abrasive milling operation, part 1: Prediction of degree of milling. *Biosystems Engineering, 88*(3), 337–342. https://doi.org/10.1016/j.biosystemseng.2004.02.011

Mohapatra, D., & Bal, S. (2007). Effect of degree of milling on specific energy consumption, optical measurements and cooking quality of rice. *Journal of Food Engineering, 80*(1), 119–125. https://doi.org/10.1016/j.jfoodeng.2006.04.055

Monazam, E. R., Galinsky, N. L., Breault, R. W., & Bayham, S. C. (2018). Attrition of hematite particles for chemical looping combustion in a conical jet cup. *Powder Technology, 340*, 528–536. https://doi.org/10.1016/j.powtec.2018.09.027

Riley, J., Siriwardane, R., & Poston, J. (2020). Bench scale analysis of the physical attrition properties for copper-ferri-aluminate oxygen carriers during chemical looping combustion. *Powder Technology, 366*, 891–905. https://doi.org/10.1016/j.powtec.2020.02.067

Roberts, R. L. (1979). Composition and taste evaluation of rice milled to different degrees. *Journal of Food Science, 44*(1), 127–129. https://doi.org/10.1111/j.1365-2621.1979.tb10023.x

Roberts, R. L., & Wasserman, T. (1977). Effect of milling conditions on yields, milling time and energy requirements in a pilot scale Engelberg rice mill. *Journal of Food Science, 42*(3), 802–803. https://doi.org/10.1111/j.1365-2621.1977.tb12607.x

Rosenbaum, T., Tan, L., Dummeldinger, M., Mitchell, N., & Engstrom, J. (2019). Population balance modeling to predict particle size distribution upon scale-up of a combined antisolvent and cooling crystallization of an active pharmaceutical ingredient. *Organic Process Research & Development, 23*(12), 2666–2677. https://doi.org/10.1021/acs.oprd.9b00348

Samadder, M., Someswararao, C. H., & Das, S. K. (2017). Optimization of operational parameters in a cyclone type pneumatic rice polisher. *Journal of Food Processing & Technology, 8*(2). https://doi.org/10.4172/2157-7110.1000655

Vishwakarma, R. K., Shivhare, U. S., & Nanda, S. K. (2012). Predicting guar seed splitting by compression between two plates using hertz theory of contact stresses. *Journal of Food Science, 77*(9). https://doi.org/10.1111/j.1750-3841.2012.02861.x

Weerasekara, N. S., Liu, L. X., & Powell, M. S. (2016). Estimating energy in grinding using DEM modelling. *Minerals Engineering, 85*, 23–33. https://doi.org/10.1016/j.mineng.2015.10.013

Xu, W., DeCroix, D. S., & Sun, X. (2014). Mechanistic based DEM simulation of particle attrition in a jet cup. *Powder Technology, 253*, 385–392. https://doi.org/10.1016/j.powtec.2013.11.031

Yan, T. Y., Hong, J. H., & Chung, J. H. (2005). An improved method for the production of white rice with embryo in a vertical mill. *Biosystems Engineering, 92*(3), 317–323. https://doi.org/10.1016/j.biosystemseng.2005.07.014

Zeng, Y., Jia, F., Chen, P., Qiu, H., Han, Y., Meng, X., et al. (2019). Effects of convex rib height on spherical particle milling in a lab-scale horizontal rice mill. *Powder Technology, 342*. https://doi.org/10.1016/j.powtec.2018.09.097

Zeng, Y., Jia, F., Meng, X., Han, Y., & Xiao, Y. (2018). The effects of friction characteristic of particle on milling process in a horizontal rice mill. *Advanced Powder Technology, 29*(5), 1280—1291. https://doi.org/10.1016/J.APT.2018.02.021

Zhang, F., Zhao, C., Guo, W., & Han, Z. (2010). Testing of grain hardness based on indentation loading curve. *Transactions of the Chinese Society of Agricultural Engineering, 41*(4), 128—133. https://doi.org/10.3969/j.issn.1000-1298.2010.04.027